BIOLOGICAL CRYSTALLOGRAPHY

ISSN 1399-0047

Structural and functional analysis of Hikeshi, a new nuclear transport receptor of Hsp70s

Jinsue Song,[a] Shingo Kose,[b]* Ai Watanabe,[b] Se-Young Son,[a] Saehae Choi,[a] Hyerim Hong,[a] Eiki Yamashita,[c] Il Yeong Park,[a] Naoko Imamoto[b]* and Soo Jae Lee[a]*

[a]College of Pharmacy, Chungbuk National University, 48 Gaeshin-dong, Heungduk-gu, Cheongju, Chungbuk 361-763, Republic of Korea, [b]Cellular Dynamics Laboratory, RIKEN, 2-1 Hirosawa, Wako, Saitama 351-0198, Japan, and [c]Institute for Protein Research, Osaka University, 3-2 Yamada-oka, Suita, Osaka 565-0871, Japan. *Correspondence e-mail: skose@riken.jp, nimamoto@riken.jp, sjlee@chungbuk.ac.kr

Received 31 July 2014
Accepted 8 December 2014

Keywords: Hikeshi; asymmetric homodimer; nuclear transport receptor; 70 kDa heat-shock proteins; FG-nucleoporins.

PDB references: Hikeshi, 3wvz; F97A mutant, 3ww0

Supporting information: this article has supporting information at journals.iucr.org/d

Hikeshi is a nuclear transport receptor required for cell survival after stress. It mediates heat-shock-induced nuclear import of 70 kDa heat-shock proteins (Hsp70s) through interactions with FG-nucleoporins (FG-Nups), which are proteins in nuclear pore complexes (NPCs). Here, the crystal structure of human Hikeshi is presented at 1.8 Å resolution. Hikeshi forms an asymmetric homodimer that is responsible for the interaction with Hsp70s. The asymmetry of Hikeshi arises from the distinct conformation of the C-terminal domain (CTD) and the flexibility of the linker regions of each monomer. Structure-guided mutational analyses showed that both the flexible linker region and the CTD are important for nuclear import of Hsp70. Pull-down assays revealed that only full-length Hsp70s can interact with Hikeshi. The N-terminal domain (NTD) consists of a jelly-roll/β-sandwich fold structure which contains hydrophobic pockets involved in FG-Nup recognition. A unique extended loop (E-loop) in the NTD is likely to regulate the interactions of Hikeshi with FG-Nups. The crystal structure of Hikeshi explains how Hikeshi participates in the regulation of nuclear import through the recognition of FG-Nups and which part of Hikeshi affects its binding to Hsp70. This study is the first to yield structural insight into this highly unique import receptor.

1. Introduction

A variety of cellular stresses affect multiple aspects of cellular physiology, including nucleocytoplasmic trafficking of macromolecules. Although it forms part of the overall regulation of trafficking, stress-induced signalling is responsible for the modulation of nuclear transport (Miyamoto *et al.*, 2004; Furuta *et al.*, 2004). During thermal stress, the level of molecular chaperones known as heat-shock proteins (Hsps) is increased to maintain the physiological homeostasis of the cell, which is an important requirement for cell survival (Wang *et al.*, 2004; Ellis & van der Vies, 1991; Mathew & Morimoto, 1998). Hsp70s (70 kDa heat-shock proteins), a major family of molecular chaperones, are involved in the highly conserved protective system, including protein folding, assembly, translocation, heterogeneous protein aggregation, signal transduction and transcriptional activation (Kampinga & Craig, 2010; Mayer, 2010). The specific roles of Hsp70s are likely to be determined by their various subcellular localizations, by the differential expression of Hsp70s at different stages of development or by their interaction with specific sets of Hsp70-associated proteins (Wang *et al.*, 2004). Following heat shock, there is a marked increase in Hsp70 production, and much of this Hsp70 rapidly migrates to the cell nucleus and becomes concentrated in the nucleoli (Welch & Feramisco, 1984; Pelham, 1984; Zeng *et al.*, 2004). Upon recovery from heat

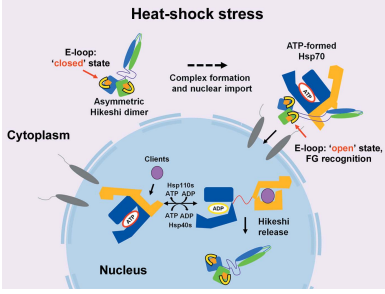

shock, the Hsp70 slowly returns to the cytoplasm. Although this phenomenon had been described many years ago, its mechanism, especially the nuclear function of Hsp70s during heat-shock stress, is only beginning to be deciphered (Zeng *et al.*, 2004).

Recently, the novel protein Hikeshi, which is essential for thermal stress-induced nuclear import of Hsp70s, was identified (Kose *et al.*, 2012). Under non-stress conditions, many types of cargoes migrate between the nucleus and the cytoplasm with the aid of the importin–Ran system (Imamoto & Kose, 2012). Importin β superfamily-dependent transport cooperates with the GTPase cycle of the small GTPase Ran (Görlich & Kutay, 1999; Weis, 2003; Stewart, 2007). On the other hand, Hikeshi transport is unique because it is not driven by the GTPase cycle of Ran. Instead, Hikeshi transport requires an ATPase cycle of Hsp70s modulated by its co-chaperones. Hikeshi binds to ATP-bound Hsp70s and dissociates from the ADP-bound form. Such a binding property is proposed to be essential for the directionality of the transport (Kose *et al.*, 2012). Hikeshi shares a key feature as a nuclear transport receptor (NTR): passage through the channels of nuclear pore complexes (NPCs) embedded in the nuclear envelope (Kose *et al.*, 2012; Imamoto & Kose, 2012). NPCs are large supramolecular assemblies composed of multiple copies of approximately 30 different proteins called nucleoporins (Nups). Phenylalanine–glycine repeat-containing Nups (FG-Nups) are important for mediating both the movement of cargo–carrier complexes through NPCs and for excluding other macromolecules from the central transport channel of NPCs (Stewart, 2007). FG-Nups have a specific feature, the highly unstructured FG sequence repeat, which is commonly FG, GLFG or F*x*FG (where *x* is usually a small residue such as Ser, Gly or Ala; Tran & Wente, 2006; Rout & Wente, 1994; Rout *et al.*, 2000; Cronshaw *et al.*, 2002). The movement of cargo-bound NTRs through the NPCs requires interactions between the given NTR and a specialized subset of FG-Nups (Terry & Wente, 2007; Cook *et al.*, 2007; Milles & Lemke, 2011). The physical interactions between NTRs and FG peptides have been structurally analyzed for importin β, Ntf2 and Nxt1. In these NTRs, the Phe of an FG repeat is found in hydrophobic pockets on the protein surface of NTRs (Bayliss, Kent *et al.*, 2000; Bayliss, Littlewood *et al.*, 2000, 2002; Bayliss, Leung *et al.*, 2002; Fribourg *et al.*, 2001). Kose and coworkers showed that Hikeshi also binds directly to FG-Nups and translocates through NPCs. Here, we report the first crystal structure of full-length human Hikeshi. Hikeshi formed a novel, asymmetric homodimer induced by the linker region and an intrinsically flexible (not disordered) C-terminal domain (CTD). This asymmetric conformation seemed to be an important regulator of Hsp70 binding. The extended loop (E-loop) comprising residues Ser85–Pro106 in the N-terminal domain (NTD) covered the hydrophobic pocket effectively to shield it from the solvent. The movement of an E-loop containing the Phe97 residue could play an intervening role in recognizing an FG repeat sequence in our crystal structure. In addition, GFP-fused Phe97Ala mutants facilitated NPC passage compared with the wild type (wt) in digitonin-permeabilized HeLa cells. The functionality of the determined crystal structure was confirmed by a reconstituted transport assay using proteins generated by structure-based mutagenesis. To obtain insights into how Hikeshi specifically recognizes the ATP-bound Hsp70, we aimed to identify the binding site of Hsp70 that is required for interaction with Hikeshi. These observations provided the structural framework underlying the Hikeshi-mediated nuclear transport pathway.

2. Materials and methods

2.1. Protein expression, purification and mutagenesis

The cDNA coding for full-length human Hikeshi was cloned into pGEX-6P-1 vector and expressed in *Escherichia coli* BL21 (DE3) cells (Stratagene). Cultures were grown to an OD_{600} of ∼0.5 at 37°C and induced with 0.1 m*M* IPTG for ∼15 h at 18°C in LB medium. Hikeshi was purified using Glutathione Sepharose 4B. After removal of the GST tag, Hikeshi was further purified using Mono Q anion-exchange and Superdex 200 size-exclusion columns (GE Life Sciences). The purified protein was concentrated to 10 mg ml^{-1} in 20 m*M* Tris–HCl pH 8.0, 50 m*M* NaCl, 1 m*M* DTT. The expression protocol for selenomethionine-labelled (SeMet) protein was modified from Van Duyne *et al.* (1993). Human Hikeshi mutants were generated using the Muta-direct Site-directed Mutagenesis Kit (Intron). All constructs were sequenced by Solgent Co., Republic of Korea. SeMet and mutant Hikeshi proteins were purified as previously described for wt Hikeshi protein. For the preparation of other proteins, refer to the Supporting Information.

2.2. Crystallization and structure determination

Crystallization was performed by the vapour-diffusion method using 1 µl protein solution and an equal volume of reservoir solution at 20°C. DTT (50 m*M*) was added to the Hikeshi protein for crystallization. Crystals were obtained using a reservoir solution consisting of 0.1 *M* Tris–HCl pH 7.4, 1 *M* ammonium sulfate. The cryoprotectant solution for cooling crystals consisted of 0.1 *M* Tris–HCl pH 7.4, 1.5 *M* ammonium sulfate, 30%(*v*/*v*) glycerol. The native and SeMet crystals belonged to space group $C222_1$ (Table 1). All data sets were collected at 90 K and a wavelength of 1.00 Å on the BL44XU beamline at SPring-8, Hyogo, Japan. All data were processed with *HKL*-2000 (Otwinowski & Minor, 1997).

Initial phases for wt Hikeshi were calculated by the SAD method using an SeMet data set in *PHENIX AutoSol* (Awad *et al.*, 2008; Adams *et al.*, 2010). The final model was completed by iterative cycles of restrained refinement with *PHENIX* and manual model building with *Coot* (Emsley & Cowtan, 2004), resulting in a model with an *R* factor of 20.8% (R_{free} of 23.1%) at 1.8 Å resolution for the native data set. Ramachandran analysis showed 99.4 and 0.6% of the protein residues to be in the favoured region and the allowed region, respectively. The initial phase of the Phe97Ala mutant was obtained by the molecular-replacement method using the structure of wt Hikeshi as a search model. 99.4% of all residues were within

Table 1
Data-collection, phasing and refinement statistics.

Values in parentheses are for the highest resolution shell.

	Wild type (native)	Wild type (SeMet)	Phe97Ala (native)
Data collection			
Space group	$C222_1$	$C222_1$	$P32$
Unit-cell parameters			
a (Å)	61.1	60.8	85.7
b (Å)	137.8	139.4	85.7
c (Å)	97.9	99.1	69.1
$\alpha = \beta$ (°)	90.0	90.0	90.0
γ (°)	90.0	90.0	120.0
Wavelength (Å)	0.9192	0.9792	0.9192
Resolution (Å)	39.9–1.88	50.0–3.11	50.0–2.50
$R_{\rm merge}$†	0.076 (0.45)	0.094 (0.65)	0.072 (0.66)
$\langle I/\sigma(I)\rangle$	66.0 (7.9)	6.6 (2.3)	10.2 (1.3)
Completeness (%)	99.1 (99.8)	100 (100)	99.8 (100)
Average multiplicity	12.1	8.0 (8.3)	3.9 (3.9)
Refinement			
Resolution (Å)	39.9–1.88		42.7–2.50
No. of reflections (work/free)	32074/1697		18451/994
$R_{\rm work}/R_{\rm free}$‡ (%)	20.7/22.8		19.5/22.4
No. of atoms			
Protein	2871		2719
Water	226		69
B factors (Å^2)			
Protein	41.5		53.8
Water	48.1		50.0
R.m.s. deviations§			
Bond lengths (Å)	0.005		0.003
Bond angles (°)	0.865		0.735

† $R_{\rm merge} = \sum_{hkl}\sum_i |I_i(hkl) - \langle I(hkl)\rangle| / \sum_{hkl}\sum_i I_i(hkl)$. ‡ $R_{\rm work} = \sum_{hkl} ||F_{\rm obs}| - |F_{\rm calc}|| / \sum_{hkl} |F_{\rm obs}|$, where $R_{\rm free}$ is calculated for a randomly chosen 5% of reflections which were not used for structure refinement and $R_{\rm work}$ is calculated for the remaining reflections. § R.m.s. deviations are from ideal values (Engh & Huber, 1991).

the Ramachandran favoured or allowed regions for the Phe97Ala mutant structure, with 0.6% as outliers. Data-collection and refinement statistics are shown in Table 1. Structural figures were prepared using *PyMOL* (http://www.pymol.org). Models were superposed using the procedure implemented in *Coot* and *PyMOL* and the relevant root-mean-square deviations for C^{α} atoms were calculated. Analysis of the dimer interface and the accessible surface area (ASA) was performed by *PISA* in the *CCP*4 package (Winn *et al.*, 2011) and the *Protein Interactions Calculator* website (http://crick.mbu.iisc.ernet.in/~PIC; Tina *et al.*, 2007).

2.3. CD spectrum analysis

The secondary-structure contents of the wt and mutants were analyzed by CD spectroscopy with a J815 spectrometer using 0.1 cm light-path cuvettes (Jasco). The purified proteins were analyzed at a concentration of 1–0.5 mg ml^{-1} in 10 m*M* sodium phosphate pH 7.5. Wavelength scans were monitored from 250 to 190 nm with ten averages.

2.4. *In vitro* nuclear transport assay

Digitonin-permeabilized HeLa-S3 cells and Imps-depleted cytosol were prepared as described previously (Kose *et al.*, 2012). Nuclear 6×His-ProS2-FLAG-Hikeshi proteins were detected by indirect immune fluorescence. After the import reactions, the cells were fixed in 3.7% formaldehyde in transport buffer for 5 min at room temperature and permeabilized with 0.2% Triton X-100 in phosphate-buffered saline (PBS) for 5 min at room temperature. After blocking with 3% skimmed milk in PBS, the cells were incubated with rabbit anti-FLAG monoclonal antibodies (Sigma) for 1 h at room temperature and detected with Alexa Fluor 488-labelled goat anti-rabbit antibodies (Molecular Probes). Fluorescent images were recorded using an Olympus BX51 microscope and an ORCA-ER camera (Hamamatsu) controlled by the *MetaVue* software (Universal Imaging). The fluorescence intensities of each nuclear protein were measured with the *ImageJ* software.

2.5. Pull-down binding assay

As described in the figure legends, recombinant proteins, 1 m*M* ATP or Imps-depleted cytosol were rotated with Phenyl Sepharose (low substitution; GE Healthcare) in 1 m*M* DTT in TB for 1 h at 4°C. The beads were spun down and washed three times with 1 m*M* DTT in TB. The bound proteins were eluted with SDS–PAGE sample buffer. After SDS–PAGE (12% polyacrylamide gels), the proteins were stained with Coomassie Brilliant Blue (CBB) or detected by immunoblotting with mouse 1H5-1 monoclonal antibodies (specific to Hsc70/Hsp70), mouse anti-FLAG monoclonal antibodies (Sigma) and HRP-conjugated secondary antibodies (Bio-Rad) using the ECL technique.

3. Results

3.1. Overall structure

Here, we report the crystal structure of full-length Hikeshi solved by MAD techniques at 1.8 Å resolution. The full data-collection and refinement statistics are shown in Table 1. The final model included a dimer per crystallographic asymmetric unit (consisting of residues 1–195 for monomer *A*) with a total of 226 water molecules (Fig. 1*a*). The disordered residues 61–64, 133–135 and 196–197 of monomer *A* and 60–63, 86–94, 98–106 and 197 of monomer *B* were omitted from the model because of poor electron density. We confirmed the dimeric arrangement of Hikeshi in solution using size-exclusion chromatography (Supplementary Fig. S5*a*); this corresponded to the crystal state, implying that the dimeric structure might be a functional unit. Each monomer (*A* and *B*) showed that the NTD with the E-loop and the CTD were joined by a flexible linker region (Fig. 1*a*). Similar search results for the Hikeshi structure with the *DALI* server (Holm & Sander, 1998) revealed a very low degree of structural similarity to other protein structures. The closest structural relative was β-agarase 1 (PDB entry 2cdp; Henshaw *et al.*, 2006), with a *Z*-score of 5.9. Sequence comparisons revealed that except in yeast, Hikeshi proteins generally share greater than 70% sequence identity and 80% similarity (without insertions or deletions), which would inevitably confer great structural similarity. *Schizosaccharomyces pombe* Hikeshi, which showed similar biochemical properties to human Hikeshi (Oda *et al.*, 2014), had high sequence similarity to human

Hikeshi. On the other hand, *Saccharomyces cerevisiae* Hikeshi (OPI10_YEAST; 6% sequence identity and 19% similarity, with a large insertion) may have some different structural elements (Supplementary Fig. S1). As illustrated in Fig. 1(*a*), Hikeshi is a domain-crossed, asymmetric homodimer with a flexible linker in the middle. The secondary structure of the monomer included nine β-strands and four α-helices (Fig. 1*b*). The NTD (residues 1–123) contained a jelly-roll/β-sandwich fold comprising two layers of antiparallel β-sheets consisting of three (β1, β4 and β7) and five (β2, β3, β5, β6 and β8) antiparallel β-strands, respectively (Supplementary Fig. S1*c*), which was somewhat different from the general β-sandwich with two layers of four-stranded β-sheets. It seemed that the E-loop of monomer *A* could be traced because of its interaction with a neighbouring NTD in the crystal (Fig. 1*c*). However, only His95, Pro96 and Phe97 were visible among the 22 amino acids in the E-loop of monomer *B* (Supplementary Fig. S2*d*). The E-loop linking antiparallel β-sheets (β7 and β8) was located at one edge of the fold across the concave face formed by β2, β3, β5 and β6 and closed over the hydrophobic pocket, which was otherwise effectively shielded from the solvent (Figs. 1*c* and 4*a*). Specifically, residue Phe97 was fully

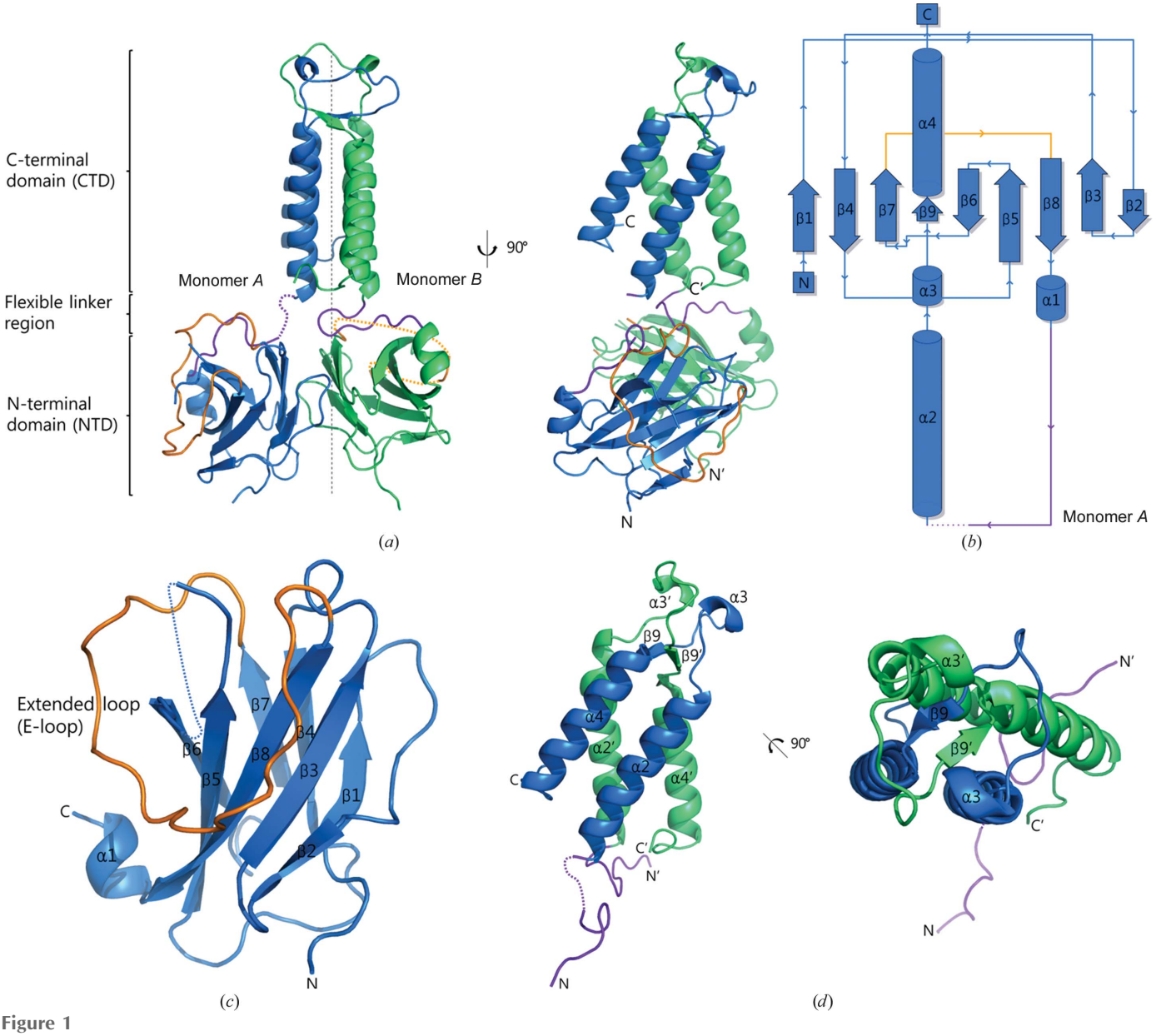

Figure 1
Overall fold and topology of the Hikeshi structure. (*a*) Ribbon representation of an asymmetric dimer structure. The vertical dotted line divides monomers *A* (marine blue) and *B* (lime green) on the left and right. The linker region and the E-loop are coloured purple and orange, respectively. (*b*) The fold of Hikeshi is represented by a topology diagram. The colour code of the secondary-structure elements is the same as in monomer *A*. (*c*) The NTD (coloured as in Fig. 1*a*) resembles the well known jelly-roll/β-sandwich fold. The strand labels are the same as in Fig. 1(*b*). The disordered region is schematically shown as a dotted line. The E-loop is discussed in the text. (*d*) Front and top views of the CTD. The CTD exhibits a coiled-coil-like conformation. Dotted lines represent disordered regions which are only present in the flexible linker region of monomer *A*. Two CTDs are crossed with an angle of about ∼40° (left) and the flexible segments containing the short β9 and α3 of each monomer show a domain crossover (right).

buried in the hydrophobic pocket, which resembled the FG repeat binding site as an anchor point. A flexible linker region (residues 124–134) connecting the NTD to the CTD was fully traced in monomer *B* but was partially disordered in monomer *A*. The CTDs of monomers *A* and *B* (residues 135–195) included three α-helices (α2, α3 and α4) and a short β-strand (β9), respectively, and showed a coiled-coil-like conformation in which two antiparallel helices were connected by a flexible segment containing the short β9 and α3 (Fig. 1*d*). A series of hydrophobic interactions and hydrogen bonds between the side chains of residues Val135–Trp195 contributed to the intramolecular interface of the two antiparallel helices α2 and α4 (Supplementary Fig. S2*a*).

3.2. Asymmetric arrangement of the Hikeshi dimer

The Hikeshi structure displayed a unique asymmetric homodimer formed *via* an extensive dimer interface mediated by theNTD and CTD of each monomer. Ubiquitous transporter importins act as monomers and the mRNA transporter TAP creates a heterodimer with p15 (Teplova *et al.*, 2011). The RanGDP transporter NTF2 forms a 'symmetric' homodimer which is clearly different from Hikeshi. The two NTD monomers of Hikeshi were aligned with the overall pseudo-twofold axis, where residues Leu5, Val11, Val37, Phe39 and Ile81 from each monomer formed the hydrophobic core. This hydrophobic core provided a dimer interface, resulting in stabilization of the rigid dimer arrangement (Fig. 2*a*). The driving force for dimerization *via* the CTD was attributed to the exclusion of solvent *via* multiple hydrophobic contacts within two pairs of antiparallel helices, comprised of α2 and α4 from each monomer, crossing each other at an angle of ~40° (Fig. 1*d*). The angle was close to the value of 50° typically encountered in helix–helix packing in globular proteins, but different from the angle of 20° observed in four-helix bundles (Chothia *et al.*, 1981). Residues Phe141, Phe149 and Phe171 made extensive contacts with the opposing monomer in a symmetric manner (Fig. 2*b*). In particular, residue Phe141 was fully buried within the hydrophobic core formed by residues Phe138, Phe141, Phe184 and Trp195 on another monomer (Supplementary Fig. S2*b*). Additionally, the turn–α3–turn–β9 segment (residues 156–173) connecting helices 2 and 4 of each monomer showed a domain crossover and was intimately intertwined (Figs. 1*d* and 2*b*, left). Because the domain-crossed structure seemed to be unusual, we carefully validated the structure. The coordinates around the domain crossing of each monomer were well fitted in the experimentally phased map at 1.8 Å resolution (Supplementary Fig. S2*c*). Three residues (Phe171–Pro173) within β9 of each monomer participated in intermolecular contacts. In particular, Phe171 made hydrophobic interactions with Val158, Phe171 and Pro173 from the opposing β9 (Fig. 2*b*, left). The dimer interface was also stabilized by hydrogen bonds between the side chains of residues Asn148, Glu169, Asn175 and Trp180 (Fig. 2*b*, middle and right). The dimer interface *via* the CTD made extensive contacts with a buried area of 3820 Å^2 out of a total buried area of 7250 Å^2.

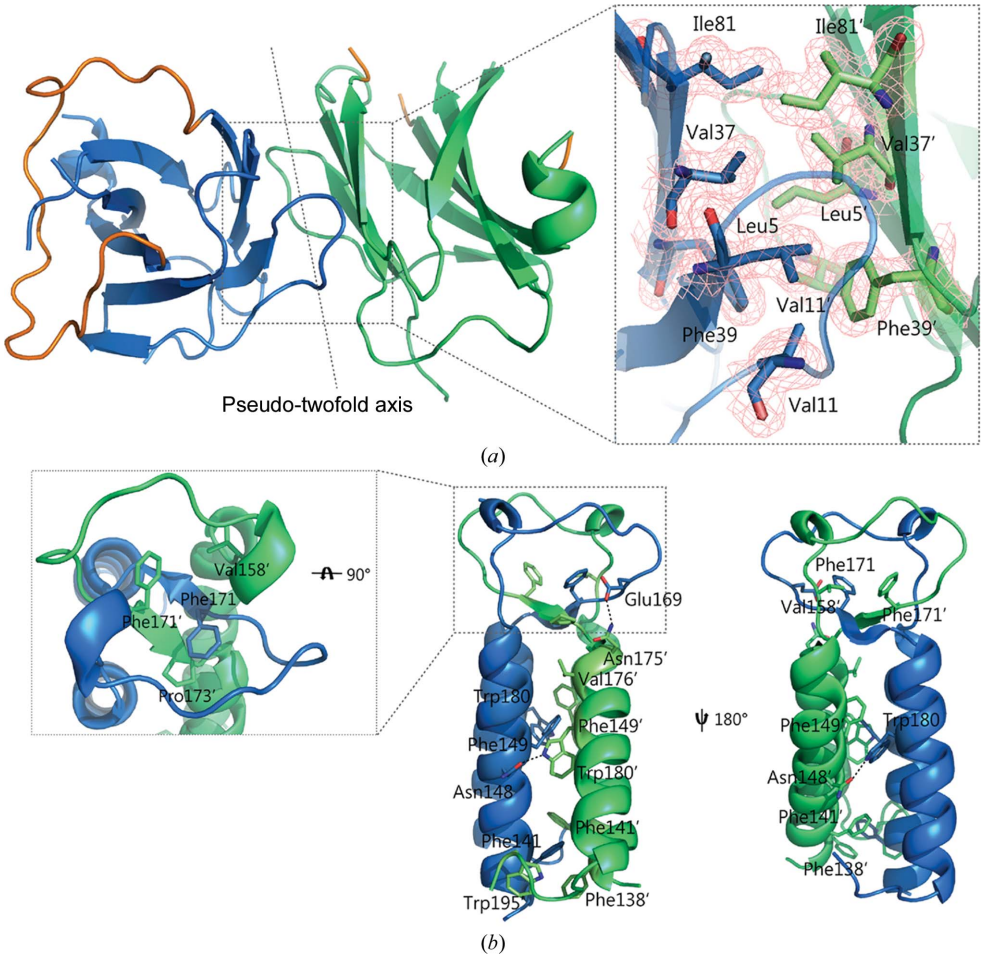

Figure 2
Structural basis for the dimerization. (*a*) Close-up view of the NTD dimeric interface contact along the pseudo-twofold axis. The side chains of Leu5, Val11, Val37, Phe39 and Ile81 located in pseudo-symmetrical positions, which form the hydrophobic cavity, are also shown as sticks (O, red; N, blue). $2|F_o| - |F_c|$ maps (pink mesh) are contoured at 1.0σ. (*b*) Arrangement of the dimer interface between the CTDs (coloured as in Fig. 1*a*). The side chains of crucial interacting residues are shown as sticks. Hydrogen bonds are indicated by dotted lines. Left, interactions of the intertwined helix 3–β-sheet 9–turn segment from each monomer. Middle, interaction between helices 2 and 4 of the two monomers. Right, a flipped view of the same structure related by a rotation of approximately 180°.

The hydrophobic interactions in the dimer interface *via* the CTD are listed in Supplementary Table S1.

Although the secondary structure of each monomer in the Hikeshi dimer was essentially identical, the relative spatial positioning of the two monomers differed significantly in our crystal structure. Superposition of monomers *A* and *B* underlined the distinct conformations of the two monomers, and there was a large root-mean-square deviation (r.m.s.d.) of about 6.7 Å (for 193 C^{α} atoms). In addition, the distances between the Ala19 and Ala161 C^{α} atoms in each monomer at each end of the longest axis of the molecule were 69.6 and 75.2 Å, respectively, reflecting distinct conformations of the monomers in the dimer (Supplementary Fig. S3*a*). While the NTDs of the two monomers were almost identical to each other, with an r.m.s.d. of 0.5 Å over 123 C^{α} atoms (Supplementary Fig. S3*b*), the CTDs showed a remarkable difference, with a large r.m.s.d. of 3.1 Å over 60 C^{α} atoms (Supplementary Fig. S3*c*). The distinct conformation of the CTDs was created by the mobility of the turn–α3–turn–β9 segment connecting helices 2 and 4, leading to different angles between the secondary-structure elements in the two monomers. Additionally, the flexible linker region connecting the NTD to the CTD seemed to be another element that allowed the spatially distinct arrangement of each monomer. The flexible linker may allow a relatively free motion of the NTD and the CTD, which could induce asymmetry of the dimer. Taken together, the distinct conformation of the CTDs and the flexibility of the linker regions connecting the NTD and the CTD appeared to lead to asymmetry in the Hikeshi homodimer. The type and number of amino acids were common to the dimer interfaces of the wt and Phe97Ala mutant crystal structures, although the structure of the CTDs in the wt and the Phe97Ala mutant showed a high r.m.s.d. (3.05 Å for 60 C^{α} atoms). In addition, the asymmetric dimer interface was identical in the two different crystal lattices of the wt and the Phe97Ala mutant, confirming that it was not a crystal-packing artifact (Supplementary Fig. S6).

3.3. Functional significance of the asymmetric dimer in Hsp70 binding

Previous studies showed that Hikeshi physically interacted with Hsp70s in a pull-down assay from cell extracts, mediating the nuclear import of Hsp70s either in the presence of cell extracts or if the Hsp70s were fixed in the ATP-bound form (Kose *et al.*, 2012). Some studies of the asymmetry of homodimeric proteins have shown that asymmetric homodimers have an adaptive property for the recognition of corresponding partners. To assess the functional significance of the asymmetric dimer of Hikeshi in Hsp70 recognition, we performed a nuclear import assay and a pull-down assay using deletion and alanine mutants of Hikeshi. These structure-based mutants were designed on the basis of the dimer interface of the CTD, including the flexible linker region, which affected the asymmetric conformation. A nuclear import assay with GFP-fused Hsc70 in digitonin-permeabilized cells revealed that the Phe141Ala mutant, a Val132–Val135 internal deletion (Δ132–135) and the Lys77Ala mutant showed reduced nuclear import activity (Fig. 3*a*). The Phe141Ala mutant lacked the buried phenyl ring within the hydrophobic core formed by residues Phe138, Phe141, Phe184

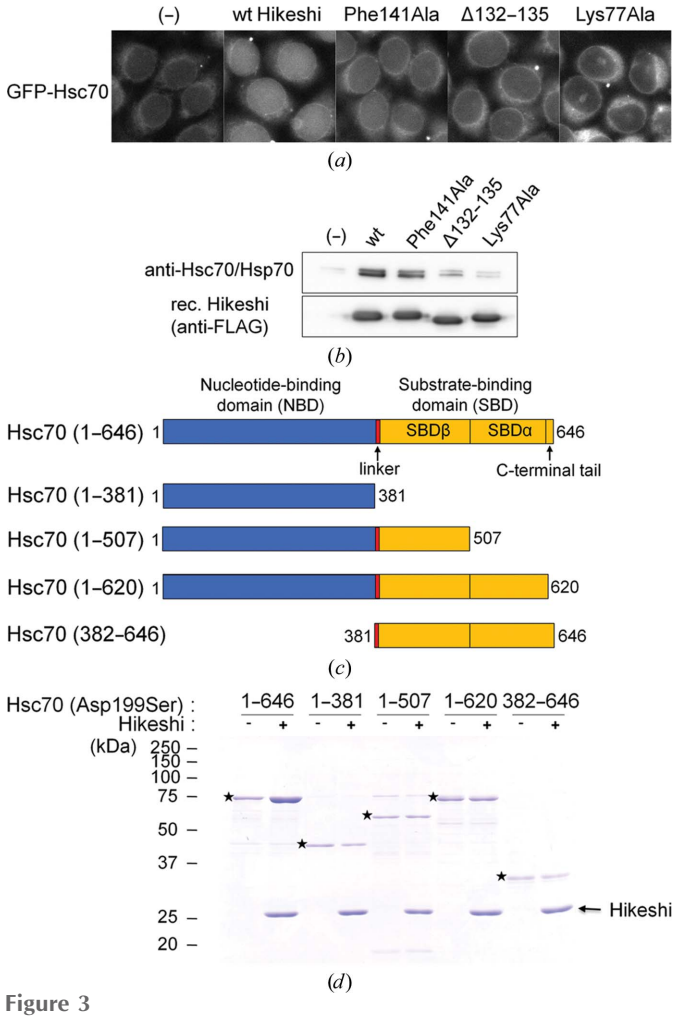

Figure 3
The asymmetric dimer is important for the binding and nuclear import of Hsp70. (*a*) Hikeshi mutants (Phe141Ala, Δ132–135 or Lys77Ala) show reduced levels of nuclear import activity of Hsc70. Semi-intact cells were incubated with GFP-Hsc70, importins (Imps)-depleted cytosol and an ATP-regenerating system in the presence or absence of recombinant wt Hikeshi or its mutant proteins for 20 min at 30°C. (*b*) Hikeshi mutants (Phe141Ala, Δ132–135 or Lys77Ala) bind less strongly to Hsc70/Hsp70. The Imps-depleted cytosol was incubated with or without recombinant FLAG-tagged wt Hikeshi or its mutant proteins and then subjected to pull-down assays with Phenyl Sepharose. Hsp70s and recombinant Hikeshi proteins were detected by immunoblotting with anti-Hsp70s and anti-FLAG antibodies, respectively. (*c*) Schematic representation of the Hsc70 constructs. The nucleotide-binding domain (NBD), linker and substrate-binding domain (SBD) are shown in blue, red and yellow, respectively. (*d*) Full-length Hsc70 is required for Hikeshi binding. His_6-tagged Hsc70 (ATPase-deficient mutant; Asp199Ser) fragments and 1 m*M* ATP were incubated with or without recombinant Hikeshi proteins. Hikeshi-interacting Hsc70 fragments were co-precipitated with Phenyl Sepharose, subjected to SDS–PAGE and detected with CBB staining. The His_6-tagged Hsc70 (ATPase-deficient mutant; Asp199Ser) fragments were the full length (residues 1–646), the N-terminal (residues 1–389) and C-terminal (residues 390–646) regions, which have been reported to contain the NBD and SBD, respectively, residues 1–507 and residues 1–620. Only full-length Hsc70 (Asp199Ser) bound purified Hikeshi. A star indicates bands that were nonspecifically binding.

and Trp195 from another monomer (Supplementary Fig. S2*b*) and Δ132–135 reduced the free motion in the flexible linker region. The Lys77Ala mutant, which was positioned in the loops connecting strands β6 and β7 close to the flexible linker region and exposed to the solvent, most effectively decreased the nuclear import activity. Lys77 was also one of the most conserved residues among Hikeshi proteins from different species. A solvent-exposed Lys77 located on the same surface as the flexible linker region (Supplementary Fig. S4*a*) might be involved in modulating the stability of the formation of the Hikeshi–Hsc70 complex. Although the above three mutants did not disrupt the dimer formation of Hikeshi in solution (Supplementary Fig. S5*a*), these mutations markedly impaired binding to Hsc70 (Fig. 3*b*). Also,

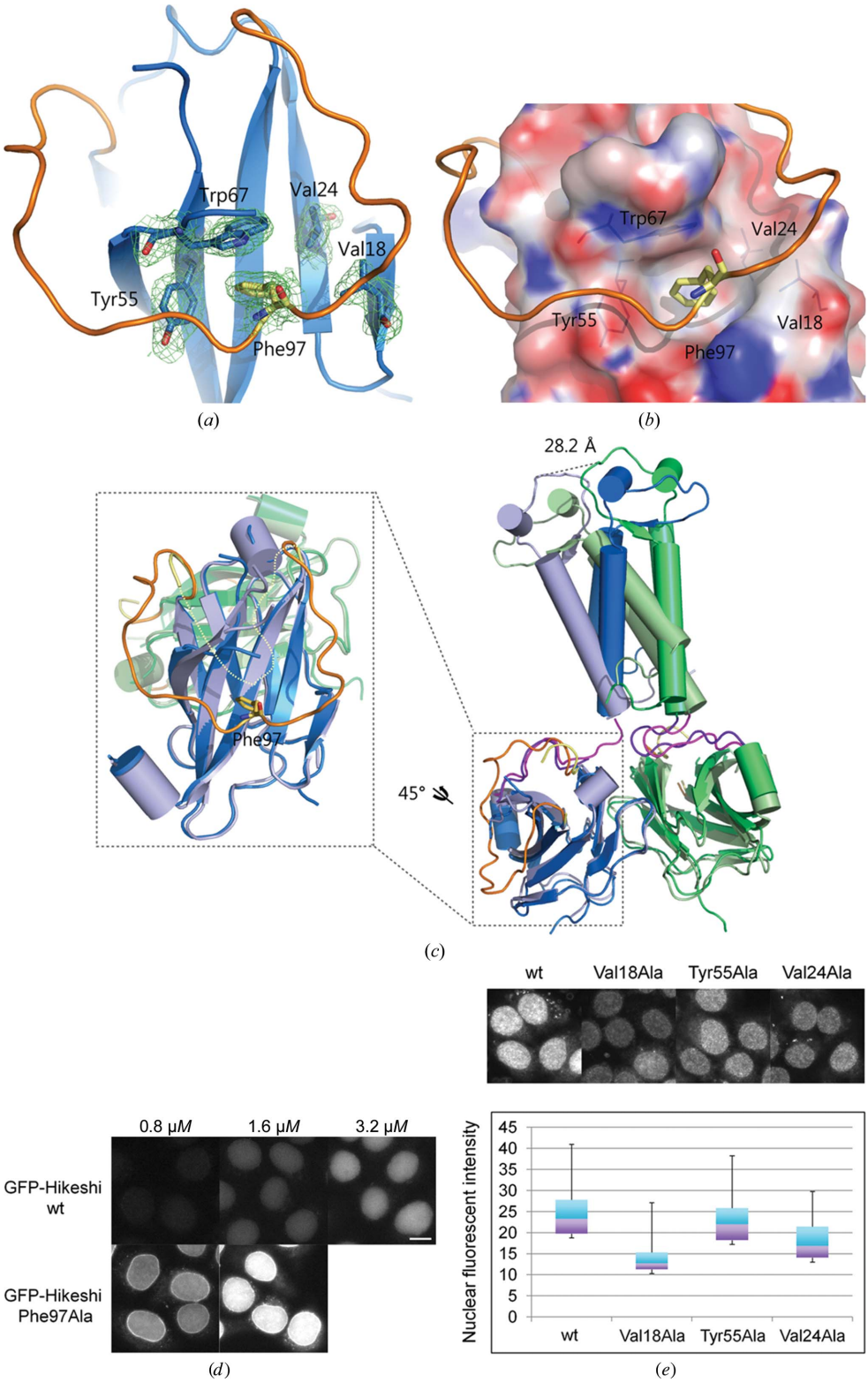

Figure 4
The E-loop is responsible for the regulation of nuclear import through the control of FG-repeat recognition. (*a*) View of the E-loop (cartoon representation) fully traced on one surface of the NTD. Phe97 is fully buried in the hydrophobic pocket and resembles the FG repeat binding site. $2|F_o| - |F_c|$ maps (green mesh) are contoured at 1.0σ. The key residues are shown as sticks (O, red; N, blue). (*b*) Electrostatic surface representation showing the hydrophobic pocket with the bound Phe97 residue of Hikeshi. The surface is coloured according to the electrostatic potential and viewed in an orientation similar to (*a*), with negatively charged areas shown in red and positively charged areas shown in blue. (*c*) Superposition of the Phe97Ala mutant on the wt. The colour code of the wt is the same as that in Fig. 1(*a*). Slate blue, NTD; light green, CTD; magenta, flexible linker; light yellow, E-loop in the Phe97Ala mutant structure. The Phe97Ala structure shows a drastic conformational change. The r.m.s.d. of the two structures is 5.3 Å for overall C^{α} atoms. The E-loop of Phe97Ala mutant was largely disordered. The hydrophobic pocket of Phe97Ala is exposed to the solvent. The disordered region is schematically shown as a dotted line. (*d*) The Phe97Ala mutant increases the activity for NPC passage compared with the wt. Recombinant wt GFP-Hikeshi or Phe97Ala mutant proteins at the concentrations indicated in the figure were incubated with semi-intact cells for 10 min at 30°C. The scale bar is 10 µm in length. (*e*) The Hikeshi single mutants Val18Ala, Val24Ala and Tyr55Ala reduce the activity of NPC passage compared with the wt. Recombinant His6-ProS2-FLAG-tagged Hikeshi or its mutant proteins (molecular weight 50 kDa), which are too large to diffuse passively into the nucleus, were incubated with semi-intact cells for 10 min at 30°C. Nuclear Hikeshi proteins were detected by indirect immunofluorescence using anti-FLAG antibodies. Nuclear fluorescence intensities were measured with *ImageJ* and their distributions are presented as box-and-whisker plots.

as shown in Supplementary Fig. S5(*b*), all of the mutants had circular-dichroism (CD) spectra similar to that of the wt, indicating that the mutations had little influence on the secondary structure of Hikeshi. We thus consider that the mutations disturbed the stability of the asymmetric conformation of the Hikeshi dimer without affecting the secondary structure of Hikeshi, leading to an interruption in the stable formation of the Hikeshi–Hsp70 complex. Therefore, we consider that the asymmetric dimer of Hikeshi might be essential for binding to Hsp70.

3.4. Full-length Hsp70 is required for Hikeshi binding

Although it has been shown that Hikeshi preferentially binds to ATP-bound Hsp70s but not to ADP-bound Hsp70s (Kose *et al.*, 2012), the interacting regions between Hikeshi and Hsp70 remain to be elucidated. With the purified Hikeshi and a series of His_6-fused Hsc70 fragments (an ATPase-deficient point mutant; Asp199Ser; Fig. 3*c*; Wilbanks *et al.*, 1994), we attempted to map the interaction domain of Hsc70 required for Hikeshi binding with *in vitro* pull-down assays. Interestingly, the full-length Hsc70 (Asp199Ser) efficiently bound to purified Hikeshi (Fig. 3*d*), whereas all other Hsc70 fragments failed to bind to purified Hikeshi. Such results differed from any of the reported interactions with Hsp70; co-chaperones such as Hsp110 (Schuermann *et al.*, 2008), Hsp40 (Suh *et al.*, 1998) and Bags (Sondermann *et al.*, 2001) interacted with the nucleotide-binding domain (NBD) of Hsp70, whereas unfolded substrates interacted with the substrate-binding domain (SBD; Awad *et al.*, 2008). According to a recently reported model for the allosteric opening of the ATP-form Hsp70, upon ATP–ADP exchange Hsp70 was converted into the ATP-bound state and the NBD and SBD formed extensive contacts which led to large conformational changes in the SBD (Qi *et al.*, 2013). As a result, Hikeshi might have the possibility of recognizing conformational changes by ADP–ATP exchange of Hsp70 molecules rather than a certain region.

3.5. The E-loop plays a critical role in regulation of the binding of FG-Nups and NPC translocation

The E-loop in the NTD was highly exposed on its surface and exhibited a fully extended conformation (Figs. 1*a* and 1*c*). Surface-exposed loops often play key roles in the functions of a protein (Skliros *et al.*, 2012). Uniquely, the phenyl ring of Phe97 in the core of the E-loop was coordinated in the hydrophobic pocket that was formed by residues Val18, Val24, Tyr55 and Trp67 (Fig. 4*a*). The interaction was dominated by hydrophobic contacts between the phenyl ring of Phe97 and residues making a hydrophobic pocket. We also observed that a side-chain C^{β} atom of Phe97 was deeply buried in a hydrophobic pocket (Fig. 4*b*), in contrast to the rest of the E-loop, and covered the hydrophobic pocket like a lid, effectively shielding it from solvent and resulting in the rigidity of an extended and flexible conformation of the loop (as seen in monomer *A*). Hikeshi bound to FG-Nups and translocated through NPCs that drive the nuclear import of Hsp70 under heat-shock conditions. The interaction between Phe97 and residues forming the hydrophobic pocket was similar to the recognition of the nucleoporin Phe residue by other NTRs (Bayliss, Littlewood *et al.*, 2000; Bayliss, Leung *et al.*, 2002; Fribourg *et al.*, 2001; Grant *et al.*, 2003). To investigate whether the conformation of the Phe97 residue plays an important role in NPC passage, we replaced Phe97 with an alanine, solved the crystal structure of the Phe97Ala mutant at 2.5 Å resolution (Table 1) and examined the ability of the Phe97Ala mutant to pass through the NPC. The overall fold of the Phe97Ala mutant protein structure underwent a drastic 'conformational change' that might be induced by a flexible linker connecting the NTD and CTD, based on the resulting superposition between Phe97Ala and wt protein (Fig. 4*c*). The overall C^{α} r.m.s.d. of Phe97Ala indicated a significant difference compared with the wt protein at 5.3 Å, while the NTD and CTD of Phe97Ala both showed high overall topological similarity, with C^{α} r.m.s.d.s of 0.57 Å (Supplementary Fig. S4*b*) and 0.45 Å (Supplementary Fig. S4*c*), respectively. These results indicated that the flexible linker connecting the NTD and CTD possessed a large structural motion, which affected the dynamic movement of Hikeshi. In particular, the distance between the C^{α} atom of Pro165, one of the residues in the turn–α3–turn–β9 segment of CTDs, in the wt and the Phe97Ala mutant was 28.2 Å (Fig. 4*c*). The E-loop containing the Phe97Ala mutation was largely disordered in both monomers, in contrast to the same loop of the wt (Fig. 4*c*), indicating that Phe97 was responsible for the decreased flexibility of the E-loop as an anchor point (see §4). In addition, GFP-fused Phe97Ala definitely showed an increase in NPC passage compared with the wt in digitonin-permeabilized HeLa cells (Fig. 4*d*). These data suggested that stabilization of the 'closed' hydrophobic pocket conformation by the E-loop interrupted the docking of the GLFG/F*x*FG repeat. It seems likely that the motional freedom of the E-loop is responsible for the movement of the phenyl ring of Phe97 upon hydrophobic pocket binding, which helped to provide a high priority for the GLFG/F*x*FG peptide. In addition, the results of the point mutation in the hydrophobic pocket supported the importance of the pocket for the recognition of FG-Nups and NPC translocation. GFP-fused mutants of the amino acids forming the hydrophobic pocket showed reduced levels of NPC passage compared with the wt in digitonin-permeabilized HeLa cells (Fig. 4*e*). The single mutants Val18Ala, Val24Ala and Tyr55Ala weakened the nuclear import activity of Hikeshi. In particular, the Val18Ala mutation impaired the nuclear migrating activity of Hikeshi most strongly among the mutant proteins examined. We performed CD experiments to measure the conformational stability of the mutant proteins. The CD data showed that in the same buffer conditions all of the mutant proteins did not undergo the conformational changes undergone by the wt protein (Supplementary Fig. S7). We thus consider that the loss of function of the mutants was not induced by a conformational change. Our data showed that this hydrophobic pocket participated in FG recognition. The NTD of Hikeshi provided a platform that allowed the recognition of FG-Nups for nuclear import of Hsp70.

4. Discussion

4.1. Asymmetric conformations of Hikeshi lead to the formation of a complex with Hsp70

Hikeshi, a fourth NTR after the importins, NTF2 and TAP, is essential for the heat-shock-induced nuclear import of Hsp70s (Kose *et al.*, 2012). The crystal structure of Hikeshi represents a novel fold with a unique asymmetric homodimer. The structure consisted of two domains, an NTD and a CTD, that are joined by a flexible linker region. In our structure, Hikeshi had an asymmetric dimer conformation driven by a flexible linker region and the turn–α3–turn–β9 segment of the CTD, although the dimer arrangement of both the NTD and the CTD of Hikeshi showed rigidity. Interestingly, the turn–α3–turn–β9 segment of CTD showed conformational variability (see Supplementary Fig. S3). This would allow dynamic arrangement of each monomer, leading to asymmetric conformations of Hikeshi and simultaneously increasing the overall stability of the dimer *via* domain crossover.

Our structure-based mutations, together with pull-down assays and digitonin-permeabilized cell-free transport assay data, support the possibility that an asymmetric dimer of Hikeshi may be responsible for the unique fit of the interaction with Hsp70. In particular, Δ132–135 in the flexible linker showed marked defects in both Hsc70 binding and nuclear import (Figs. 3*a* and 3*b*). The mutation of the highly conserved Lys77 to Ala, which was exposed on the same surface with the flexible linker, produced even more severe defects than Δ132–135. These data suggest that the asymmetric dimer of Hikeshi might be closely linked to its Hsp70-binding and nuclear import activity.

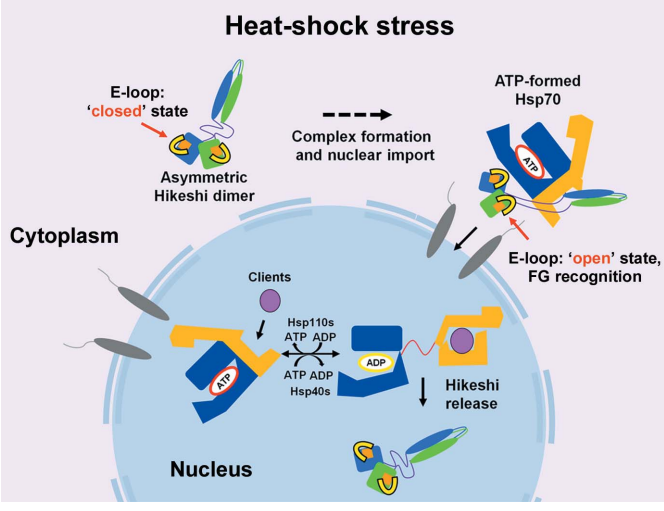

Figure 5
Schematic illustration of how Hikeshi carries Hsp70 from the cytoplasm to the nucleus through the NPCs. The asymmetric dimer of Hikeshi interacts with the ATP-formed Hsp70. The asymmetric arrangement recognizes allosteric conformation changes by ADP–ATP exchange of Hsp70 molecules and forms a binding site for complex formation. The NTD region of Hikeshi binds to components of the nuclear basket such as FG repeats. This interaction provides the NPC passage of the Hikeshi–Hsp70 complex.

Homodimers with asymmetry rarely exist (Swapna *et al.*, 2012). The asymmetric structure provides a binding site for the corresponding partner. For example, in the crystal structure of rotavirus nonstructural protein 3 (NSP3), asymmetric homodimerization enables the generation of a highly basic RNA-binding site (Piron *et al.*, 1999). The asymmetric dimer form of the C-terminus of Hsp70-interacting protein (CHIP), which is an E3 ubiquitin ligase, is also important for interaction with the ubiquitin-conjugating enzyme Ubc13 (Zhang *et al.*, 2005). The structure of HAP1, which is a member of a family of fungal transcription factors, showed that HAP1 is bound in a dramatically asymmetric manner to the DNA target (Zhang & Guarente, 1996; King *et al.*, 1999). Finally, PAN3, one of two cytoplasmic mRNA deadenylases, forms intertwined and asymmetric homodimers similar to the CTD of Hikeshi, and this asymmetry appeared to be crucial for binding PAN2 (Christie *et al.*, 2013). Taken together, our data provide the attractive possibility that the asymmetric conformation of the Hikeshi dimer has been preserved for interaction with Hsp70 under physiological conditions. However, it is not yet clear whether the asymmetric conformation is owing to rearrangement induced by the flexibility of Hikeshi or its intrinsic folds.

In the phase determination of the diffraction from wt Hikeshi and the Phe97Ala mutant, rigid-body refinement using the NTD and CTD structures of Hikeshi were sometimes not successful, although the structures were obtained from the same crystal type. These phenomena might be related to intrinsic properties of the protein such as local flexibility and deformability of each domain. The high degree of flexibility of the Hikeshi molecule seemed to be stabilized through the recruitment of binding partners such as Hsp70s. In an *in vitro* assay, the binding of Hikeshi to Hsp70 was unique because it required full-length Hsc70 (residues 1–646; Asp199Ser). Our findings suggest the possibility that Hikeshi may recognize an allosteric conformational change by ADP–ATP exchange of Hsp70 molecules rather than specific regions of Hsp70 because Hikeshi failed to bind to any of the Hsc70 fragments that were examined (Fig. 5). Hikeshi also did not bind to residues 1–620 of the Hsc70 fragment containing the SBD, which was related to conformational changes of Hsp70. The C-terminus of Hsc70 is structurally not defined; however, this portion plays a unique role as it is responsible for binding CHIP (Smith *et al.*, 2013). The requirement of the C-terminus of Hsc70 for Hikeshi binding further implied that this portion also affected the complexation of ATP-bound Hsp70 with Hikeshi.

4.2. Regulation mechanism of Hikeshi for NPC translocation of Hsp70

In general, NTRs can move their bound cargoes through NPCs by interacting with FG-Nups. We have tried to solve crystal structures of the Hikeshi–FG peptide complex, but we could not determine these structures. Previous studies have also reported that the FG-Nup binding of Hikeshi was weaker than that of importin β (Kose *et al.*, 2012). It is thought that the weakness of the interaction between Hikeshi and FG-Nups

was one reason why it was difficult to obtain crystals of the Hikeshi–FG peptide complex. The E-loop of Hikeshi plays a critical role in the regulation of FG-Nup binding and NPC translocation. Residues Phe97-Gly98 (FG) of the E-loop, which are the typically repeating FG sequences contained in FG-Nups, interrupted the docking of the GLFG/F*x*FG repeat through capping of the 'open' hydrophobic pocket conformation by the E-loop. GFP-fused Phe97Ala, which removes the phenyl group of Phe97 covering the hydrophobic pocket, showed increased levels of NPC passage compared with the wt in digitonin-permeabilized HeLa cells (Fig. 4*d*). Protein loops sometimes play important roles in protein function (Fetrow, 1995) such as participating in a binding site for interaction with another protein (Saraste *et al.*, 1990; Via *et al.*, 2000; Stuart *et al.*, 1986). We assume that Phe97 in the E-loop and the hydrophobic pocket contributed to the regulation needed for nuclear transport ability.

The hydrophobic pocket mutation diminished the NPC-passage activity of Hikeshi, as shown by a nuclear transport assay (Fig. 4*e*). In particular. the Val18Ala Hikeshi mutant resulted in a remarkable decrease in NPC passage activity. Taken together, our data suggest the following molecular basis of a potential recognition site for FG-Nups in Hikeshis. In any signalling process induced by a variety of cellular stresses, in which Hsp70s would be required to enter the nucleus and then be recognized by Hikeshi, the E-loop of Hikeshi containing Phe97 undergoes a conformational change upon Hsp70 binding. This change is a result of either induced fit or increased flexibility. The hydrophobic pocket modifies its structural conformations from a 'closed' state to an 'open' state, resulting in the binding of FG-Nups. Although the structure of the NPC in the normal cell has been well studied, little is known about the altered structure and the function of the NPC induced by cellular stresses such as heat shock.

In summary, although definite roles of Hsp70 in the nucleus are currently unknown, Hikeshi-mediated nuclear import of Hsp70 is an important part of the cellular response to stress, as nuclear Hsp70 is required for cell survival after stress damage. Asymmetric dimerization of Hikeshi is responsible for binding Hsp70, leading to nuclear import of Hsp70, and for recognizing the conformational changes on ADP–ATP exchange in Hsp70. Our data also provide information on how Hikeshi selectively recognizes FG-Nups. The transport assays support that the E-loop and hydrophobic pocket of Hikeshi participate in the recognition of FG-Nups.

5. Related literature

The following references are cited in the Supporting Information for this article: Kose *et al.* (1997).

Acknowledgements

This research was supported by a National Research Foundation of Korea (NRF) grant funded by the Korean government (MEST; 2008-0062275 and 2011-0017405 to SJL) and a Japanese Ministry of Education, Culture, Sports, Science and Technology Grant-in-Aid (to SK) and funding awarded to NI by the Japan Society for the Promotion of Science (JSPS) through the 'Funding Program for Next Generation World-Leading Researchers (NEXT Program)' initiated by the Council for Science and Technology Policy (CSTP). The synchrotron-radiation experiments were performed on BL44XU at SPring-8, Japan (2012B6500, 2013A6500 and 2013B6500) and the Protein Beamline, Pohang Light Source, Republic of Korea.

References

Adams, P. D. *et al.* (2010). *Acta Cryst.* D**66**, 213–221.
Awad, W., Estrada, I., Shen, Y. & Hendershot, L. M. (2008). *Proc. Natl Acad. Sci. USA*, **105**, 1164–1169.
Bayliss, R., Kent, H. M., Corbett, A. H. & Stewart, M. (2000). *J. Struct. Biol.* **131**, 240–247.
Bayliss, R., Leung, S. W., Baker, R. P., Quimby, B. B., Corbett, A. H. & Stewart, M. (2002). *EMBO J.* **21**, 2843–2853.
Bayliss, R., Littlewood, T. & Stewart, M. (2000). *Cell*, **102**, 99–108.
Bayliss, R., Littlewood, T., Strawn, L. A., Wente, S. R. & Stewart, M. (2002). *J. Biol. Chem.* **277**, 50597–50606.
Chothia, C., Levitt, M. & Richardson, D. (1981). *J. Mol. Biol.* **145**, 215–250.
Christie, M., Boland, A., Huntzinger, E., Weichenrieder, O. & Izaurralde, E. (2013). *Mol. Cell*, **51**, 360–373.
Cook, A., Bono, F., Jinek, M. & Conti, E. (2007). *Annu. Rev. Biochem.* **76**, 647–671.
Cronshaw, J. M., Krutchinsky, A. N., Zhang, W., Chait, B. T. & Matunis, M. J. (2002). *J. Cell Biol.* **158**, 915–927.
Ellis, R. J. & van der Vies, S. M. (1991). *Annu. Rev. Biochem.* **60**, 321–347.
Emsley, P. & Cowtan, K. (2004). *Acta Cryst.* D**60**, 2126–2132.
Engh, R. A. & Huber, R. (1991). *Acta Cryst.* A**47**, 392–400.
Fetrow, J. S. (1995). *FASEB J.* **9**, 708–717.
Fribourg, S., Braun, I. C., Izaurralde, E. & Conti, E. (2001). *Mol. Cell*, **8**, 645–656.
Furuta, M., Kose, S., Koike, M., Shimi, T., Hiraoka, Y., Yoneda, Y., Haraguchi, T. & Imamoto, N. (2004). *Genes Cells*, **9**, 429–441.
Görlich, D. & Kutay, U. (1999). *Annu. Rev. Cell Dev. Biol.* **15**, 607–660.
Grant, R. P., Neuhaus, D. & Stewart, M. (2003). *J. Mol. Biol.* **326**, 849–858.
Henshaw, J., Horne, A., Van Bueren, A. L., Money, V. A., Bolam, D. N., Czjzek, M., Ekborg, N. A., Weiner, R. M., Hutcheson, S. W., Davies, G. J., Boraston, A. B. & Gilbert, H. J. (2006). *J. Biol. Chem.* **281**, 17099–17107.
Holm, L. & Sander, C. (1998). *Nucleic Acids Res.* **26**, 316–319.
Imamoto, N. & Kose, S. (2012). *Nucleus*, **3**, 422–428.
Kampinga, H. H. & Craig, E. A. (2010). *Nature Rev. Mol. Cell Biol.* **11**, 579–592.
King, D. A., Zhang, L., Guarente, L. & Marmorstein, R. (1999). *Nature Struct. Mol. Biol.* **6**, 64–71.
Kose, S., Furuta, M. & Imamoto, N. (2012). *Cell*, **149**, 578–589.
Kose, S., Imamoto, N., Tachibana, T., Shimamoto, T. & Yoneda, Y. (1997). *J. Cell Biol.* **139**, 841–849.
Mathew, A. & Morimoto, R. I. (1998). *Ann. N. Y. Acad. Sci.* **851**, 99–111.
Mayer, M. P. (2010). *Mol. Cell*, **39**, 321–331.
Milles, S. & Lemke, E. A. (2011). *Biophys. J.* **101**, 1710–1719.
Miyamoto, Y., Saiwaki, T., Yamashita, J., Yasuda, Y., Kotera, I., Shibata, S., Shigeta, M., Hiraoka, Y., Haraguchi, T. & Yoneda, Y. (2004). *J. Cell Biol.* **165**, 617–623.
Oda, Y., Kimura, M., Kose, S., Fasken, M. B., Corbett, A. H. & Imamoto, N. (2014). *FEBS Lett.* **588**, 1899–1905.
Otwinowski, Z. & Minor, W. (1997). *Methods Enzymol.* **276**, 307–326.

Pelham, H. (1984). *EMBO J.* **3**, 3095–3100.
Piron, M., Delaunay, T., Grosclaude, J. & Poncet, D. (1999). *J. Virol.* **73**, 5411–5421.
Qi, R., Sarbeng, E. B., Liu, Q., Le, K. Q., Xu, X., Xu, H., Yang, J., Wong, J. L., Vorvis, C., Hendrickson, W. A., Zhou, L. & Liu, Q. (2013). *Nature Struct. Mol. Biol.* **20**, 900–907.
Rout, M. P., Aitchison, J. D., Suprapto, A., Hjertaas, K., Zhao, Y. & Chait, B. T. (2000). *J. Cell Biol.* **148**, 635–651.
Rout, M. P. & Wente, S. R. (1994). *Trends Cell Biol.* **4**, 357–365.
Saraste, M., Sibbald, P. R. & Wittinghofer, A. (1990). *Trends Biochem. Sci.* **15**, 430–434.
Schuermann, J. P., Jiang, J., Cuellar, J., Llorca, O., Wang, L., Gimenez, L. E., Jin, S., Taylor, A. B., Demeler, B., Morano, K. A., Hart, P. J., Valpuesta, J. M., Lafer, E. M. & Sousa, R. (2008). *Mol. Cell*, **31**, 232–243.
Skliros, A., Zimmermann, M. T., Chakraborty, D., Saraswathi, S., Katebi, A. R., Leelananda, S. P., Kloczkowski, A. & Jernigan, R. L. (2012). *Phys. Biol.* **9**, 014001.
Smith, M. C., Scaglione, K. M., Assimon, V. A., Patury, S., Thompson, A. D., Dickey, C. A., Southworth, D. R., Paulson, H. L., Gestwicki, J. E. & Zuiderweg, E. R. (2013). *Biochemistry*, **52**, 5354–5364.
Sondermann, H., Scheufler, C., Schneider, C., Hohfeld, J., Hartl, F.-U. & Moarefi, I. (2001). *Science*, **291**, 1553–1557.
Stewart, M. (2007). *Nature Rev. Mol. Cell Biol.* **8**, 195–208.
Stuart, D. I., Acharya, K., Walker, N. P. C., Smith, S. G., Lewis, M. & Phillips, D. C. (1986). *Nature Rev. Mol. Cell Biol.* **324**, 84–87.
Suh, W.-C., Burkholder, W. F., Lu, C. Z., Zhao, X., Gottesman, M. E. & Gross, C. A. (1998). *Proc. Natl Acad. Sci. USA*, **95**, 15223–15228.
Swapna, L. S., Srikeerthana, K. & Srinivasan, N. (2012). *PLoS One*, **7**, e36688.
Teplova, M., Wohlbold, L., Khin, N. W., Izaurralde, E. & Patel, D. J. (2011). *Nature Struct. Mol. Biol.* **18**, 990–998.
Terry, L. J. & Wente, S. R. (2007). *J. Cell Biol.* **178**, 1121–1132.
Tina, K., Bhadra, R. & Srinivasan, N. (2007). *Nucleic Acids Res.* **35**, W473–W476.
Tran, E. J. & Wente, S. R. (2006). *Cell*, **125**, 1041–1053.
Van Duyne, G. D., Standaert, R. F., Karplus, P. A., Schreiber, S. L. & Clardy, J. (1993). *J. Mol. Biol.* **229**, 105–124.
Via, A., Ferrè, F., Brannetti, B., Valencia, A. & Helmer-Citterich, M. (2000). *J. Mol. Biol.* **303**, 455–465.
Wang, W., Vinocur, B., Shoseyov, O. & Altman, A. (2004). *Trends Plant Sci.* **9**, 244–252.
Weis, K. (2003). *Cell*, **112**, 441–451.
Welch, W. J. & Feramisco, J. (1984). *J. Cell Biol.* **259**, 4501–4513.
Wilbanks, S. M., DeLuca-Flaherty, C. & McKay, D. B. (1994). *J. Cell Biol.* **269**, 12893–12898.
Winn, M. D. (2011). *Acta Cryst.* D**67**, 235–242.
Zeng, X.-C., Bhasin, S., Wu, X., Lee, J.-G., Maffi, S., Nichols, C. J., Lee, K. J., Taylor, J. P., Greene, L. E. & Eisenberg, E. (2004). *J. Cell Sci.* **117**, 4991–5000.
Zhang, L. & Guarente, L. (1996). *EMBO J.* **15**, 4676–4681.
Zhang, M., Windheim, M., Roe, S. M., Peggie, M., Cohen, P., Prodromou, C. & Pearl, L. H. (2005). *Mol. Cell*, **20**, 525–538.